Journal of Civil Structural Health Monitoring (2021) 11:725–743
https://doi.org/10.1007/s13349-021-00479-8

ORIGINAL PAPER

Mapping temperature contours for a long-span steel truss arch bridge based on field monitoring data

Qing-Xin Zhu[1] · Hao Wang[1] · Zi-Dong Xu[1] · Billie F. Spencer Jr.[2] · Jian-Xiao Mao[1] · Zhao-Hua Gong[3]

Received: 21 December 2020 / Revised: 3 February 2021 / Accepted: 11 March 2021 / Published online: 27 March 2021

Abstract

The temperature-induced response of long-span steel bridges can be more significant than the structural responses associated with operational loads or structural damage. These responses depend on the spatio-temporal temperature variation in bridge members, including the effective temperature and temperature difference within members. Bridges are designed to withstand the extreme temperature variations predicted for a given site. Hence, numerous studies have employed statistical analysis techniques to provide critical information for the design and maintenance of bridges during life cycles. However, the correlation between the effective temperature and temperature difference is usually ignored, which can result in inaccurate assessment of the extreme temperatures in members. In this work, the joint probability distribution for the temperature variation in a long-span steel truss arch bridge is investigated based on field monitoring data. The extreme temperature variations are mapped on contours with relevant return periods; the results show that the probability distribution of the effective temperature can be described using the normal distribution; the weighted sum of two lognormal distributions can describe the distribution of temperature difference. Moreover, extreme values of the effective temperature and temperature difference do not occur concurrently. The effective temperature and temperature difference in the structural member directly exposed to solar radiation vary significantly, while the temperature of the shaded member can be assumed uniform, which is mainly affected by air temperature. The study leads to more accurate estimation of the temperature extremes in long-span steel truss arch bridges, which is of great importance for proper design and maintenance of bridges.

Keywords Temperature · Temperature difference · Long-span steel truss arch bridge · Filed monitoring data · Joint probability distribution · Extreme temperature variation

✉ Hao Wang
wanghao1980@seu.edu.cn

Qing-Xin Zhu
xinzqx@163.com

Zi-Dong Xu
220151062@seu.edu.cn

Billie F. Spencer Jr.
bfs@illinois.edu

Jian-Xiao Mao
jx1990@seu.edu.cn

Zhao-Hua Gong
2580170672@qq.com

[1] Key Laboratory of C&PC Structures of Ministry of Education, Southeast University, Nanjing 211189, China

[2] Newmark Endowed Chair in Civil Engineering, Department of Civil and Environmental Engineering, University of Illinois at Urbana-Champaign, Urbana, IL 61801, USA

[3] China Railway Shanghai Group Corporation Limited, Shanghai 200071, China

1 Introduction

Temperature-induced responses of long-span bridges are often more significant than responses due to operational loads or structural damage [1–4]. These responses depend on the spatio-temporal temperature variation in bridge members. The spatio-temporal temperature in the structural components of bridges exhibit complex dependencies on the air temperature, solar radiation, bridge orientation, material, cross-sections, and surface conditions [5, 6]. Bridges are designed to withstand the extreme temperature variations predicted for a given site. Overestimation of the temperature extremes can lead to expensive over-designs, whereas underestimation may pose a danger to bridge safety and serviceability. Therefore, a comprehensive understanding of the temperature variation is essential for the design and maintenance of bridges, especially long-span steel bridges [7, 8]. However, obtaining an adequate representation of the

temperature extremes for the structural elements in long-span bridges is challenging, due to the aforementioned issues.

In recent years, structural health monitoring (SHM) methods have been applied in the field to investigate spatio-temporal temperatures of bridge components, as well as the associated structural responses in full-scale bridge structures [9]. In-situ temperature measurements are the most objective method in revealing the temperature variation in bridges. Numerous SHM systems have been installed on long-span bridges worldwide [10–16]. For example, a systematic SHM system was installed on the Tsing Ma Bridge to investigate the temperature variations and dominant temperature effects [8]. In addition, the temperature measurements of the Shanghai Yangtze River Bridge indicate that the vertical temperature difference between the top and bottom plates of the girder is higher than that along the transverse direction [17]. Abid et al. investigated the impact of air temperature and solar radiation on the temperature variation in concrete-encased composite girders [18]. The experimental results showed that the vertical and lateral temperature gradients are highly dependent on sun and cloud movement. Yang et al. found that the temperature variation in the Anqing Yangtze River Bridge is symmetric based on the field temperature measurements [19]. Moreover, the influences of temperature on structural responses and structural properties have been investigated extensively [20–24]. However, the critical influence factors on the temperature variation, including air temperature, solar radiation, and wind speed, vary randomly. Accurate real-time temperature variations in bridges with complex configurations under complex boundary conditions and sunlight sheltering are challenging to be predicted.

Bridge structures can be severely affected by the combination of external loads and temperature variation [25]. The extreme temperature-induced responses of large-span bridges must be considered for proper design and maintenance of bridges. The temperature variation in bridges is intrinsically time-varying, with an underlying statistical structure due to the periodically time-varying nature of solar radiation and air temperature. Hence, numerous studies have employed statistical analysis techniques to predict long-term extreme thermal loads based on limited short-term data [26–28], which would provide critical information for the design and maintenance of long-span bridges during life cycles. Wang et al. investigated the temperature variation in a steel box girder based on the temperature measurements of the Sutong Cable-stayed Bridge [29]. Results indicate that the probability distribution of the temperature can be described using the weighted sum of four normal distributions, and the temperature difference can be described by the weighted sum of one Weibull distribution and one normal distribution. In addition, the temperature difference in the Runyang Suspension Bridge can be defined using the weighted sum of one Weibull distribution and one normal distribution [26]. Accordingly, the extreme values of temperature variations can be determined using the extreme value analysis (EVA) technology [30]. The temperature variation has significant influences on structural responses and structural properties [31, 32]. Moreover, the temperature difference produces self-equilibrated stresses in structural members, even for simply supported bridges [33]. Temperature-induced responses mainly depend on the combinations of the effective temperature and temperature difference. Therefore, the temperature loads, including the maximum effective temperature, minimum effective temperature, and maximum temperature difference, are required for bridge design.

Environment parameters are often modeled stochastically; accordingly, structures are designed to withstand the rarest environmental loads. The distribution of critical environmental conditions is often studies using the environmental contour (EC) method [34–36]. The EC method is a readily and efficient approach for establishing design loads associated with the target reliability involving structural reliability techniques [37]. Accordingly, extreme environmental loads can be selected on the contour surface with relevant return periods. Li et al. established contour surfaces for the combination of wind and wave parameters [38], which reveal the exceedance probability corresponding to a return period of 50 years. Karmakar et al. estimated the long-term joint probability distribution of extreme loads for different types of offshore floating wind turbines using the EC method [39]. In addition, the most critical structural response is associated with the highest or lowest values of environmental variables, especially the environmental conditions located at the boundary of the design region [40, 41]. Therefore, the EC method is commonly used to predict long-term extreme structural responses during life cycle. Van de Lindt and Niedzwecki described the load uncertainty for structures subjected to horizontal ground motion using the EC method [42]. The earthquake is statistically characterized in terms of magnitude, site-to-source distance, and attenuation error at a specified structural period. Lystad et al. investigated the long-term root mean square (RMS) response of the Hardanger Bridge using the EC method [43]. Results showed that turbulence-induced variability has a significant impact on the moments of bridge girder. Nevertheless, the investigation on the temperature variation in steel truss arch bridges using the EC method is not available.

In this study, the temperature variation in a steel truss arch bridge is systematically investigated based on the long-term field monitoring data, focusing on developing a better understanding of the extremes of temperature variation. First, the Dashengguan Bridge and its SHM system are introduced. Then, the characteristics of the temperature and temperature difference are analyzed based on three and a

half years of temperature data. Accordingly, the probability density distributions of the effective temperature and temperature difference are calculated, which are described using the normal distribution and weighted sum of two lognormal distributions, respectively. Subsequently, the extreme of the joint probability distribution for the temperature variation in the Dashengguan Bridge is contoured using the highest density contour (HDC) method. The results enhance the understanding of the temperature variation in long-span steel truss arch bridges, which will lead to more effective design of long-span bridges.

2 Long-term monitoring data of the Dashengguan Bridge

2.1 Bridge description

The Dashengguan Bridge carries a six-lane railway cross over the Yangtze River in Jiangsu Province, China, as shown in Fig. 1. The bridge consists of a six-span continuous steel truss bridge with a span arrangement of 108 m + 192 m + 3 36 × 2 m + 192 m + 108 m. The centerline of the bridge is oriented approximately 40° anticlockwise to the north. Two lanes on the downstream side carry the Beijing–Shanghai (B–S) high-speed railway. Two lanes on the upstream side carry the Shanghai–Wuhan–Chengdu (S–W–C) quasi-high-speed railway, and the rest on the outer sides of the bridge deck carries the Nanjing Metro Line S3. Three steel trusses are used to support the main loads, which are contacted using transverse members. The main span consists of box-shaped members and H-shaped members.

2.2 The SHM system

To ensure the safety, durability, and serviceability of the Dashengguan Bridge under long-term high-speed train loads, a comprehensive SHM system has been installed on the bridge, aiming at monitoring the temperature variation and structural responses. The SHM system was installed in June 2011 and has been operating since then. The measurement cross-sections for temperature and strain are presented in Fig. 2. Two temperature sensors and two strain sensors are mounted on the middle cross-section of structural members, aiming at recording the temperature and strain variation of the member. The typical measurement points are shown in Figs. 3 and 4. The strain and temperature sensors are each labeled to indicate the type of sensor and the sensor location. The first character in the label is either S or T, indicating strain or temperature, respectively. The next two pairs of numbers in the label indicate the section and member number, respectively. Finally, for a given structural member, E and W represent whether the sensor is mounted on the east-facing or west-facing plates, respectively. For example, T0805E represents a temperature sensor mounted on the east-facing plate of the fifth member in the eighth cross-section. Note that the temperature gradients along the longitudinal direction of members are generally neglected [44, 45]. The typical temperature distribution of structural members can be described using the temperature measurements of these critical sections. The sampling frequencies of strain data and temperature are 50 Hz and 1 Hz, respectively. However, the temperature variation is small in a short time interval. The sampling frequencies of temperature

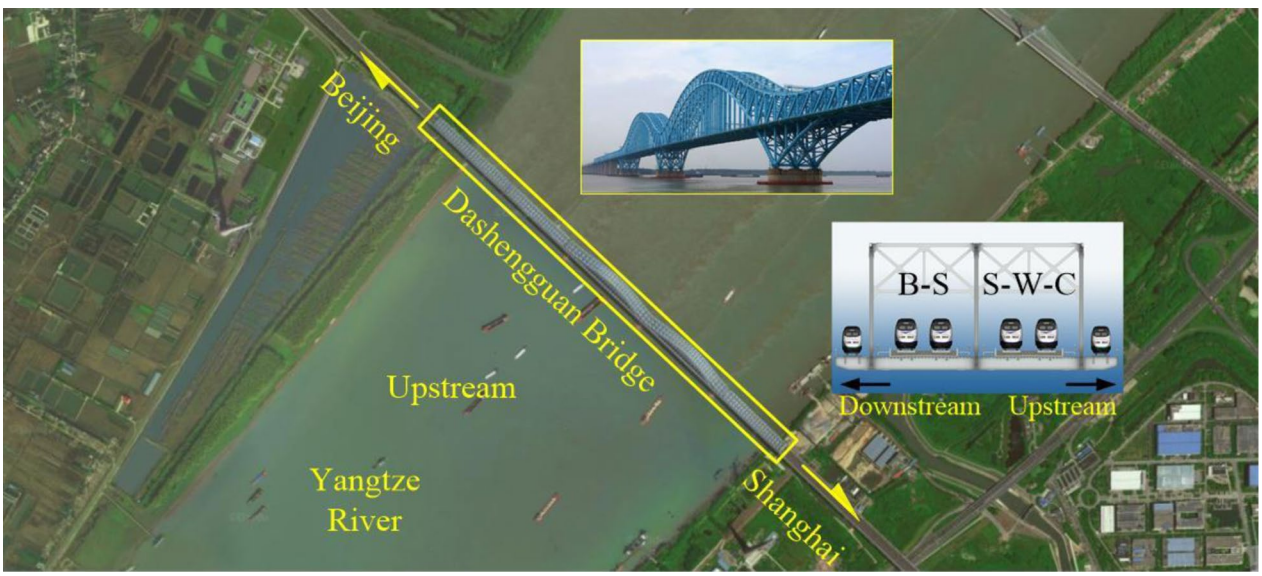

Fig. 1 Aerial view of the Dashengguan Bridge

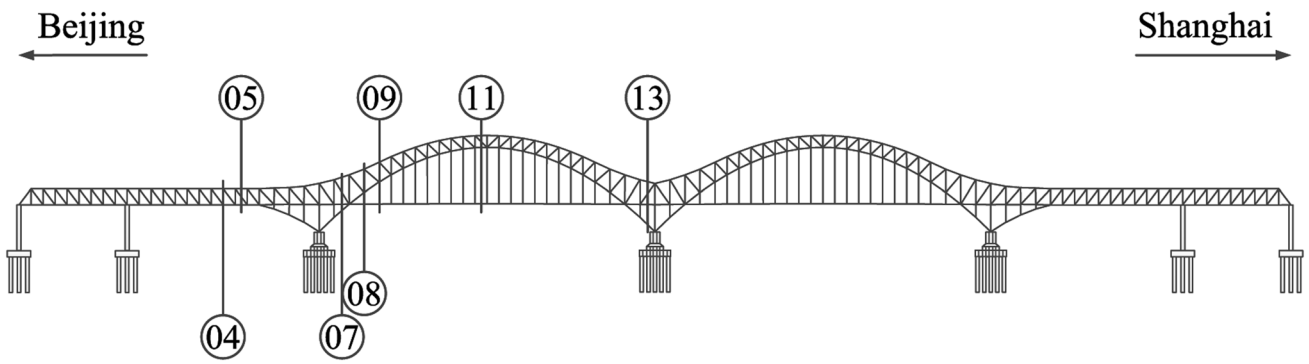

Fig. 2 Measurement cross-sections

measurements are reduced to a ten-minute average during the data processing stage.

3 Temperature measurements of the Dashengguan Bridge

Six typical kinds of structural member are utilized in the Dashengguan Bridge and are designated by *a* to *f* as follows: (a) the diagonal H-shaped member (measurement points T1105E and T1105W), (b) middle chord member (measurement points T1109E and T1109W), (c) bottom chord member (measurement points T1113E and T1113W), (d) vertical H-shaped member (measurement points T0805E and T0805W), (e) side box-shaped member under the deck (measurement points T1307E and T1307W), and (f) middle box-shaped member under the deck (measurement points T1309E and T1309W). The temperature measurements are assumed to be the similar for structural members at comparable locations under the same working conditions (e.g., the cross-sections, boundary conditions, and angle between structural member and ground) [24].

3.1 Temperature variations in the Dashengguan Bridge

The temperature measurements of the six typical structural members are shown in Fig. 5. The temperature data was recorded from January 31st, 2013 to October 30th, 2013, and August 31st, 2017 to July 8th, 2019. The temperature variations exhibit periodic behavior, corresponding to seasonal and sunlight variations. The temperature measurements reach the lowest values in January, while the highest values are recorded in July and August. In addition, significant temperature variations occur in the period from 8:00 to 20:00 each day, which are induced by solar radiation. Conversely, the temperatures change little from 20:00 to 8:00 the next day. After sunrise, the solar radiation intensity is mild, thus the temperature increases slowly during this period. About two hours after sunrise, the solar radiation increases sharply, leading to substantial warming of structural members. The solar radiation intensity starts to decrease after about 15:00; correspondingly, the temperature decreases sharply until around 20:00, because the solar heating is less than the thermal radiation from the structural member to the surroundings. After 20:00, the temperature continues to decrease gradually with the decreasing air temperature until around 8:00 the next day due to thermal convection with the surroundings.

The minimum temperature of the bottom chord member is usually higher than that of other members, because bottom chord members are protected against wind by the deck. However, there is no significant difference for the minimum temperature for the other structural members which are directly exposed to ambient air. In addition, the structural members exposed to solar radiation are easily affected by solar radiation, resulting in a notable temperature increase. Hence, the daily temperature variation of the structural members exposed to direct sunlight is higher than that of shaded structural members. Note that the peak temperature of the member under the deck occurs about two hours later than that of other members, because the temperature of members heated by the air will lag behind those heated by solar radiation.

The temperature variation of the east-facing plate shows different behavior compared to that of the west-facing plate for the first five structural members, as shown in Fig. 5a–e. During the early morning, the temperature of the east-facing plate is higher than that of the west-facing plate, because the sun rises from the east. Then, the temperature of the west-facing plate increases faster than that of the east-facing plate, due to the sun progressing toward the west. The middle box-shaped member (*f*) only receives scattered radiation during the daytime. The temperature variation can be assumed uniform, which is mainly influenced by the air temperature, as shown in Fig. 5f.

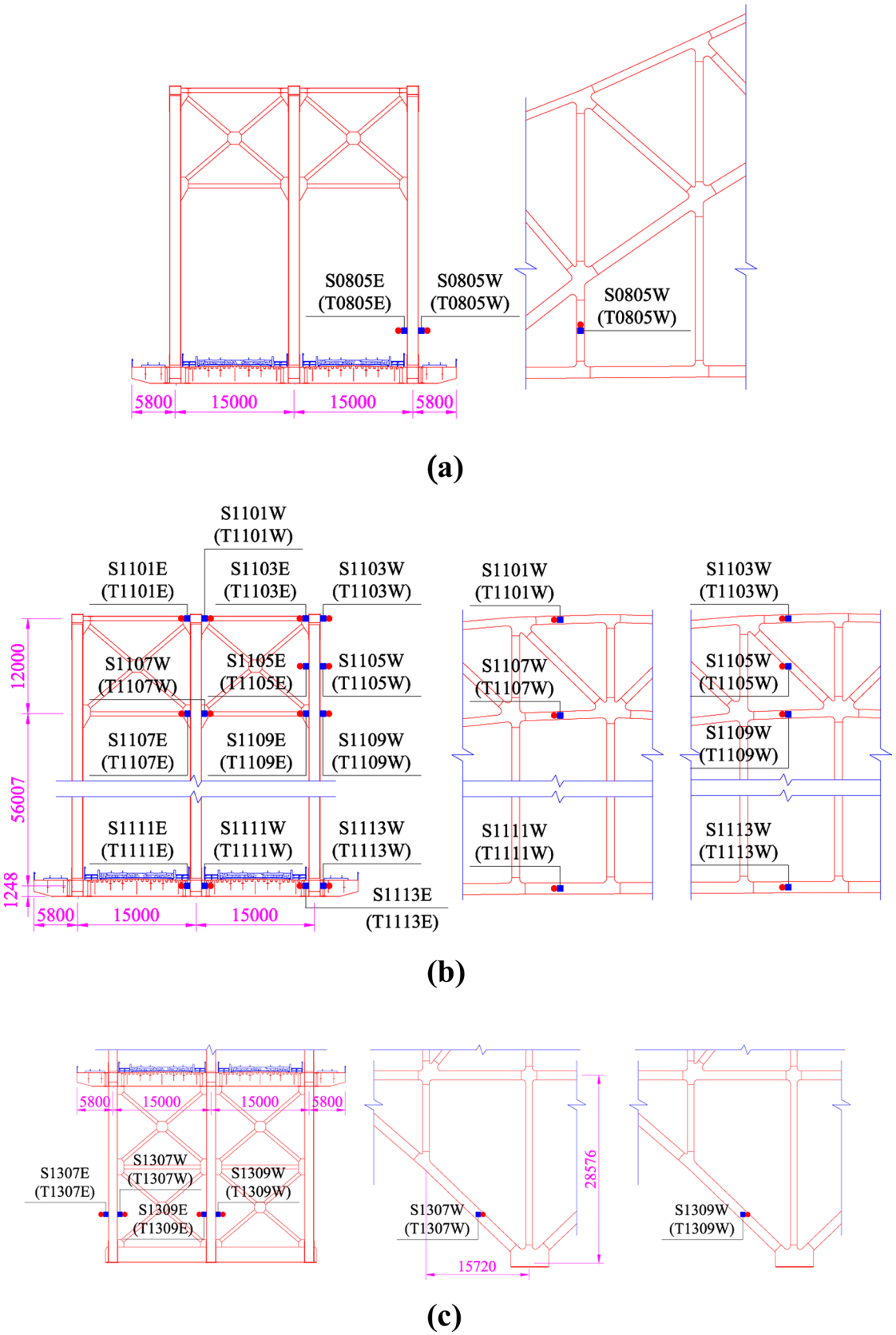

Fig. 3 Sensors layout of the SHM system (unit: mm). **a** Cross Sect. 08; **b** cross Sect. 11; **c** cross-Sect. 13

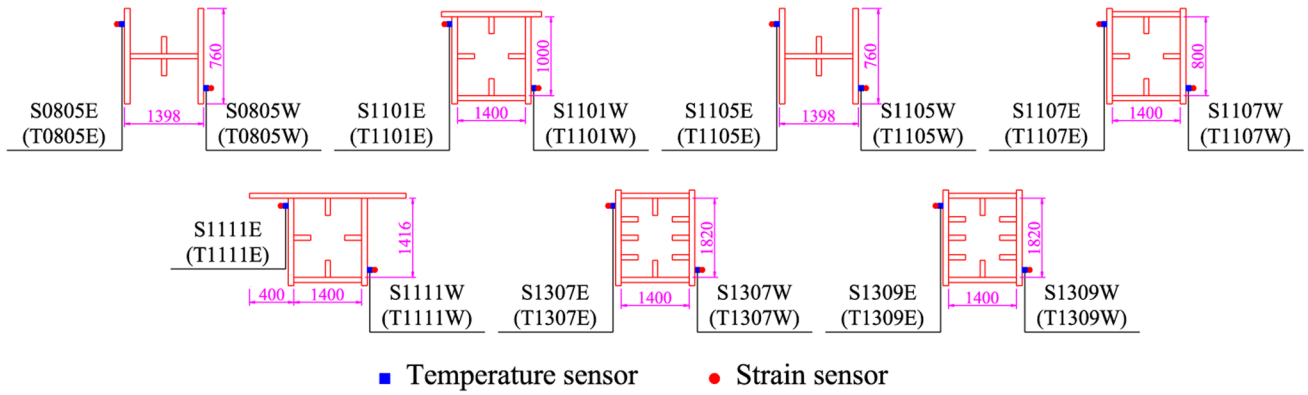

Fig. 4 Typical measurement points (unit: mm)

The temperature of the east-facing plate is higher than that of the west-facing plate for the bottom chord member in the summer, whereas the opposite situation occurs in the winter. Indeed, the summer solar radiation intensity is significantly higher than that of the winter, which warms the top plate of the deck. Hence, the temperature sensor, which is mounted on the upper part of the bottom chord member, is sensitive to the temperature variation. This phenomenon is induced by the variation of the intensity and incidence angle of solar radiation. As a result, the modest solar radiation cannot warm the top plate of the deck due to the track board on the deck, whereas the scattered radiation and air temperature provides little heat to the bottom plate of the deck. Moreover, the temperature of the east-facing plate is higher than that of the west-facing plate for the side box-shaped member during the winter daytime, as shown in Fig. 5e. The sun rises from the southeast and moves at low altitude angles to the south of the equatorial plane until setting southwest in the winter. Solar radiation can directly strike the east-facing plate, leading to a more significant temperature increase of the east-facing plate compared to the west-facing plate.

3.2 The probability density distributions of effective temperatures

The effective temperature, defined herein as the average of the temperature measured by the two sensors on the member, is used to investigate the statistical characteristic of temperature variation in structural members. The effective temperature, T_E, has significant influences on member length [46, 47] and is expected to follow a normal distribution, the probability density function (PDF) of which is given by

$$f_{T_E}(t_E)=\frac{1}{\sqrt{2\pi}\sigma_E}\exp\left[-\frac{1}{2\sigma_E^2}(x-\mu_E)^2\right], \quad (1)$$

where μ_E and σ_E are the mean and standard deviation in the normal distribution. The maximum likelihood method is employed to determine the parameters of the distributions. Figure 6 shows the empirical probability density function for the effective temperature, EPDF, which is compared to the fitted probability density function, FPDF. The empirical cumulative distribution and the fitted cumulative distribution are given by ECDF and FCDF, respectively. The parameters of the fitted effective temperature distributions are shown in Table 1. According to the Kolmogorov Smirnov (K-S) tests, the null hypotheses, which states that the effective temperature is normally distributed, cannot be rejected considering 95% confidence for (a), (b), (c), and (f), as well as 92% confidence for (d) and (e). Hence, the normal distribution is seen to provide a good model of the effective temperature data. Note that the maximum annual temperature difference in the 3.5-year period is slightly over 65 °C, which would make the main span expand nearly 1 m and result in sizeable cumulative displacements in the expansion devices and bearings.

Skewness and kurtosis describe the shape characteristics of a distribution. Skewness is a measure of symmetry, and kurtosis is a measure of whether the data are heavy-tailed or light-tailed compared to a normal distribution. For the normal distribution, the skewness is zero and the kurtosis is 3. The kurtosis and skewness calculations of effective temperatures are shown in Table 2. The skewness is close to zero, which indicates that the distribution of the effective temperature is symmetric. However, the kurtosis is smaller than expected for a normal distribution, especially the kurtosis of the vertical H-shaped member (d). This result indicates that the probability density distribution of the effective temperature is more tail heavy than the normal distribution.

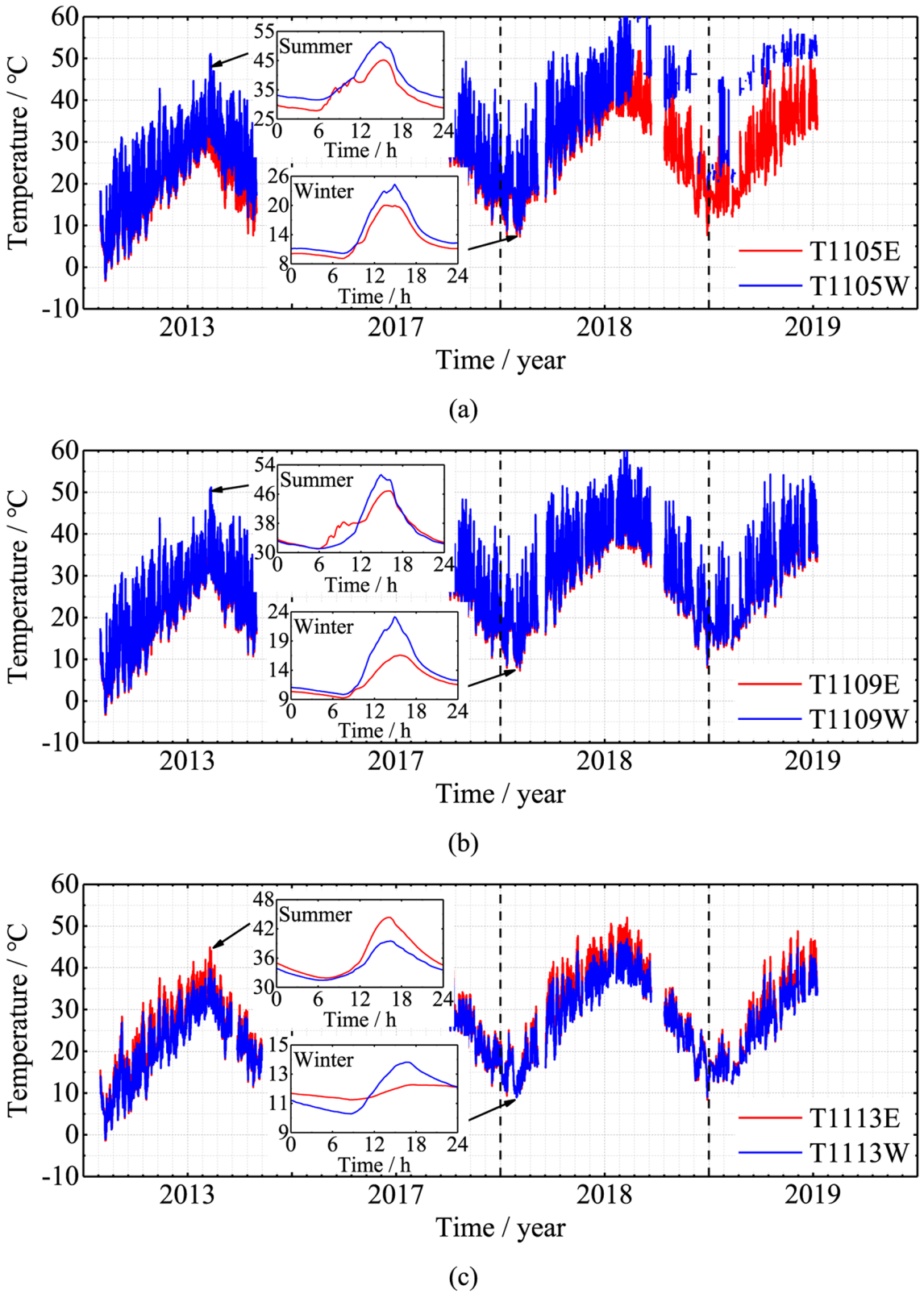

Fig. 5 Temperature variations in the Dashengguan Bridge. **a** Diagonal H-shaped member; **b** middle chord member; **c** bottom chord member; **d** vertical H-shaped member; **e** side box-shaped member; **f** middle box-shaped member

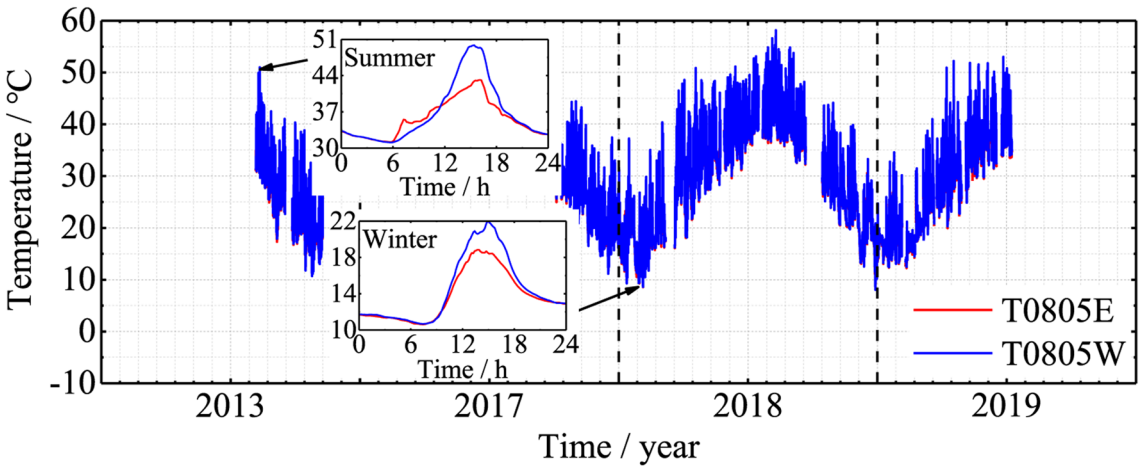

(d)

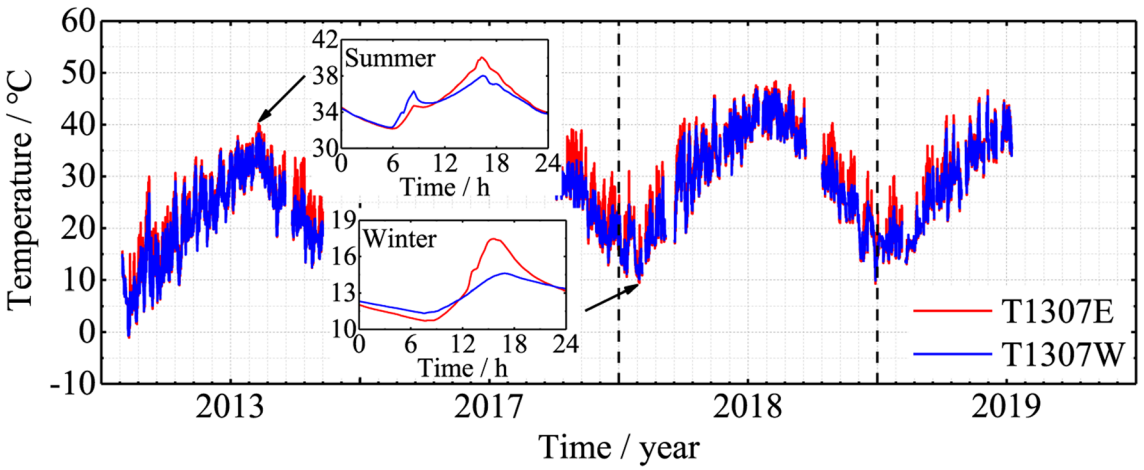

(e)

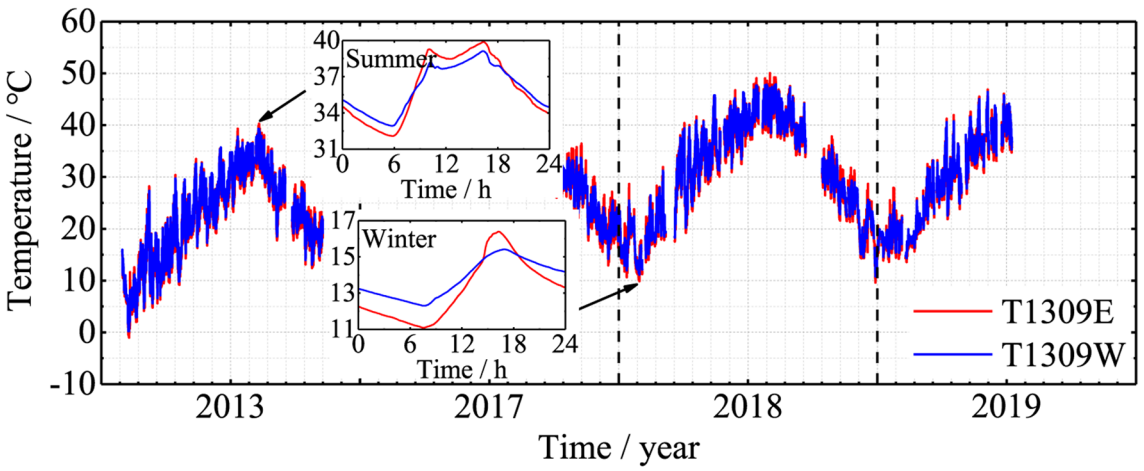

(f)

Fig. 5 (continued)

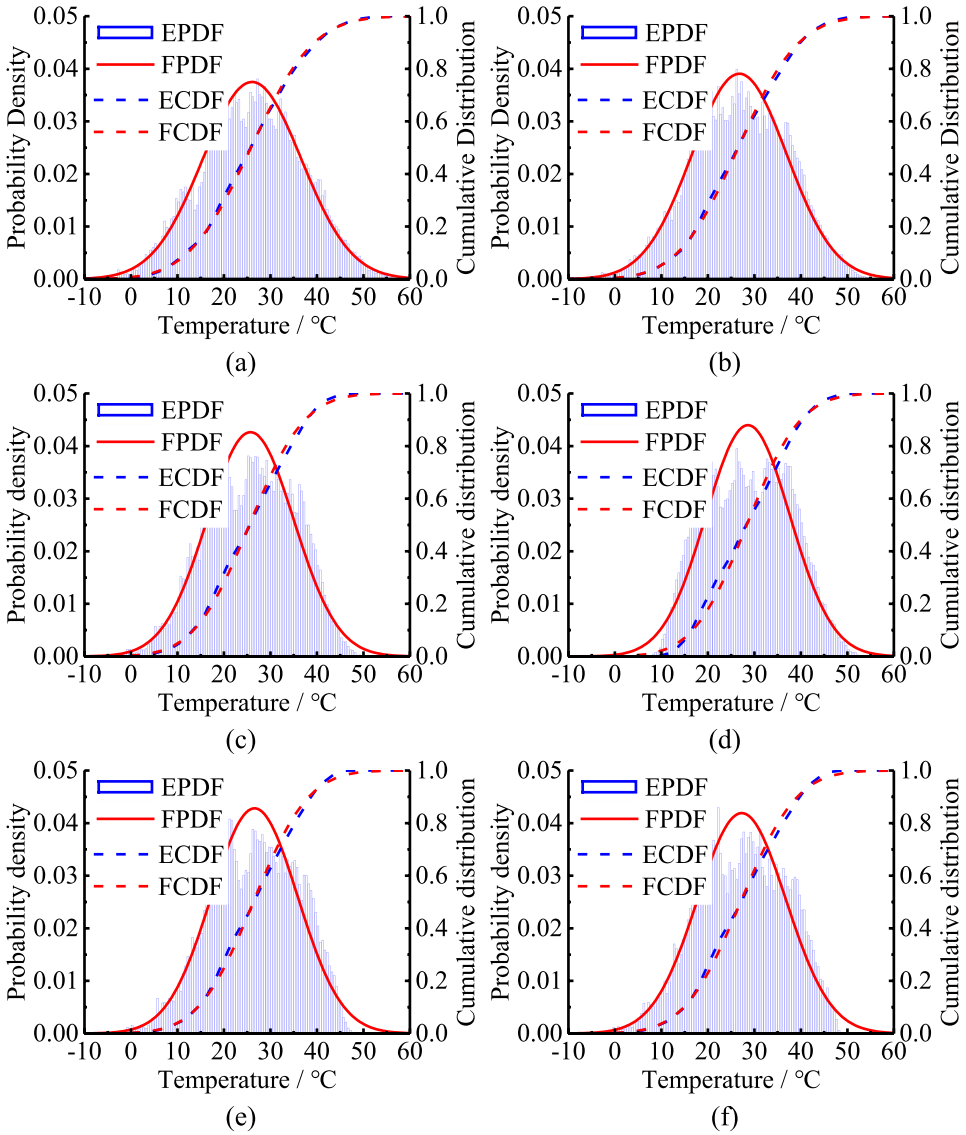

Fig. 6 Probability density functions for the effective temperature. **a** Diagonal H-shaped member; **b** middle chord member; **c** bottom chord member; **d** vertical H-shaped member; **e** side box-shaped member; **f** middle box-shaped member

Table 1 Fitting parameters of the effective temperature distributions

Structural member	a	b	c	d	e	f
Mean / ℃	26.042	26.7602	25.704	28.6056	26.5733	27.2756
Standard deviation / ℃	10.6392	10.2141	9.35415	9.07208	9.31857	9.51821

Table 2 Skewness and kurtosis of the effective temperature

Structural member	a	b	c	d	e	f
Skewness	0.024854	−0.03347	−0.07221	0.07966	−0.11885	−0.09001
Kurtosis	2.572027	2.537262	2.336661	2.089635	2.355505	2.34515

4 The temperature differences in structural members

The east-facing web plate does not receive direct solar radiation when the sun is in the west. The opposite situation occurs for the west-facing web plate when the sun is in the east. Therefore, temperature differences occur in structural members as the sun traverses the sky. Moreover, the temperature difference between the opposite plates

can be significant. The temperature difference, T_Di, of the structural member, i, is calculated as

$$T_Di = Ti\mathrm{E} - Ti\mathrm{W}, \tag{2}$$

where T_Di represents the temperature difference in structural member i, TiE and TiW represent the temperatures of the east-facing and west-facing plates of the structural member i. Accordingly, a positive temperature difference indicates that the temperature of the east-facing plate is higher than that of the west-facing plate, and vice versa.

4.1 Variations of the temperature difference in structural members

The temperature differences in the six typical structural members are shown in Fig. 7. The tendency of the temperature difference is partially correlated with the effective temperature. The temperature difference increases with increasing effective temperature during the day, whereas the temperature difference is relatively insensitive to the effective temperature during the night. The temperature difference can be characterized typically as being small before sunrise, increasing to the maximum or minimum between 14:00 and 16:00, decreasing in magnitude as the sun lowers in the sky, and finally reaching an equilibrium in the night. Note that the apparent temperature difference variation begins earlier in the summer, while it occurs later in the winter.

The daily maximum temperature difference in the middle chord member is usually higher than for other members. In contrast, the middle box-shaped member under the deck is fully shaded by the deck and is mainly influenced by ambient air; the result is that its daily maximum temperature difference is lower than other members. In addition, the daily temperature differences in the box-shaped member and the H-shaped member are more significant in the summer than in the winter. The opposite situation occurs for the box-shaped member under the deck. The east-facing plate of the box-shaped member under the deck can directly receive solar radiation due to the small incident angle of the winter solar radiation. Hence, the winter temperature difference in the member under the deck is significantly higher than that of summer. Note that the deck almost completely shades the middle box-shaped member under the deck throughout the day. Hence, the temperature distribution in the member is mainly influenced by the ambient air temperature, and the corresponding temperature difference is less than 5 °C for all seasons, as shown in Fig. 7c.

The summer temperature difference is significantly different from that of winter for the structural members directly exposed to solar radiation. The summer temperature difference consists of a peak and a valley, whereas only a valley occurs in the winter, as shown in Fig. 7a, b. The phenomenon is induced by the incident angle of solar radiation. The sun rises from the southeast and moves at low altitude angles in the winter, while the sun rises from the east and moves at high altitude angles in the summer. The east-facing plate can receive solar radiation directly during the early summer morning. In addition, a peak appears in the temperature difference of the bottom chord member in the summer, while a valley appears in the winter, as shown in Fig. 7a. The top plate of the deck is warmed substantially by solar radiation in the summer, whereas the limited solar radiation in the winter cannot warm the top plate of the deck, due to the deck being shielded by the high-speed rail track slab. The bottom plate is only affected by the ambient environmental conditions, resulting in modest variations in its temperature. Note that the temperature differences in H-shaped members share a similar tendency, as shown in Fig. 7b.

4.2 The probability density distributions of temperature differences

The combination of two lognormal distributions is employed here to describe the distribution of temperature difference, T_D. The PDF for the combination model is given by,

$$f_{T_D}(t_D)=\begin{cases} \frac{1}{\sqrt{2\pi}\sigma_{D1}(t_D-t_C)}\exp\left[-\frac{1}{2\sigma_{D1}^2}\left(\ln\left(t_D-t_C\right)-\mu_{D1}\right)^2\right] & t_D \geq t_C \\ \frac{1}{\sqrt{2\pi}\sigma_{D2}(-t_D+t_C)}\exp\left[-\frac{1}{2\sigma_{D2}^2}\left(\ln\left(-t_D+t_C\right)-\mu_{D2}\right)^2\right] & t_D < t_C \end{cases} \tag{3}$$

where σ_{D1}, μ_{D1}, σ_{D2}, and μ_{D2} are the parameters in the two lognormal distributions, including the mean and standard deviation, and t_C is the point at which T_D shifts from one lognormal distribution to another, which is corresponding to the highest probability density of the temperature difference. The fitted results for the temperature difference using the combination model are shown in Fig. 8, which are compared to the empirical probability density function. The K–S tests indicate that the assumption that the temperature difference is lognormally distributed cannot be rejected at the 95% confidence level for (c), (e), and (f), as at the 90% confidence level for (a), (b), and (d). Hence, the distribution of temperature difference is generally well approximated by the combination of two lognormal distributions. Note that two peaks appear in the empirical probability density function for the diagonal H-shaped member, as shown in Fig. 8a. The two peaks are produced by the variation of solar radiation incidence angle. The FPDF cannot describe the first peak of the EPDF, and a larger difference between the FPDF and EPDF is observed around the first peak. However, the maximum difference between the FCDF and ECDF is smaller than 0.06. Moreover, good agreement is observed between

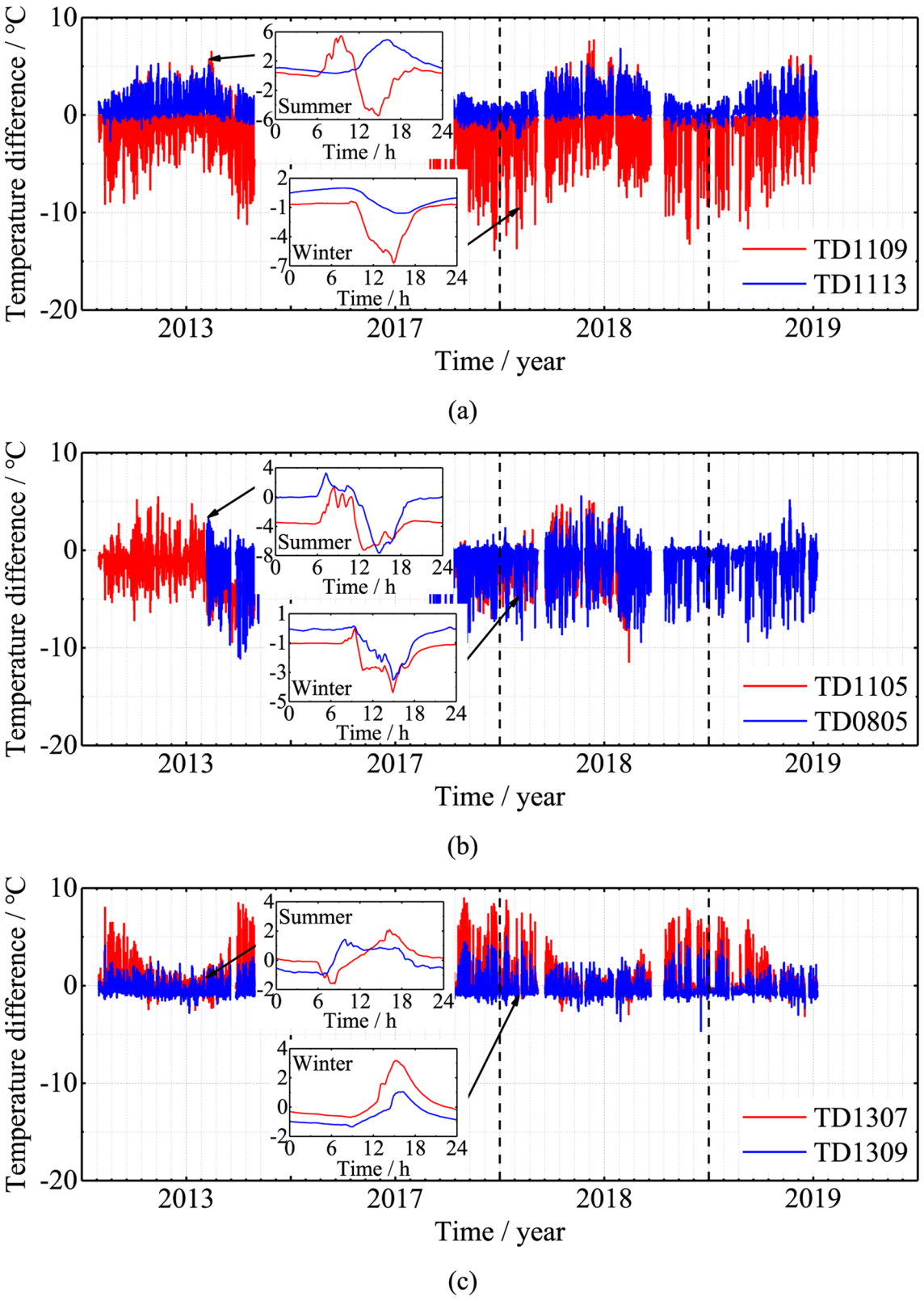

Fig. 7 Variations of temperature difference in the Dashengguan Bridge. **a** Box-shaped member; **b** H-shaped member; **c** box-shaped member under the deck

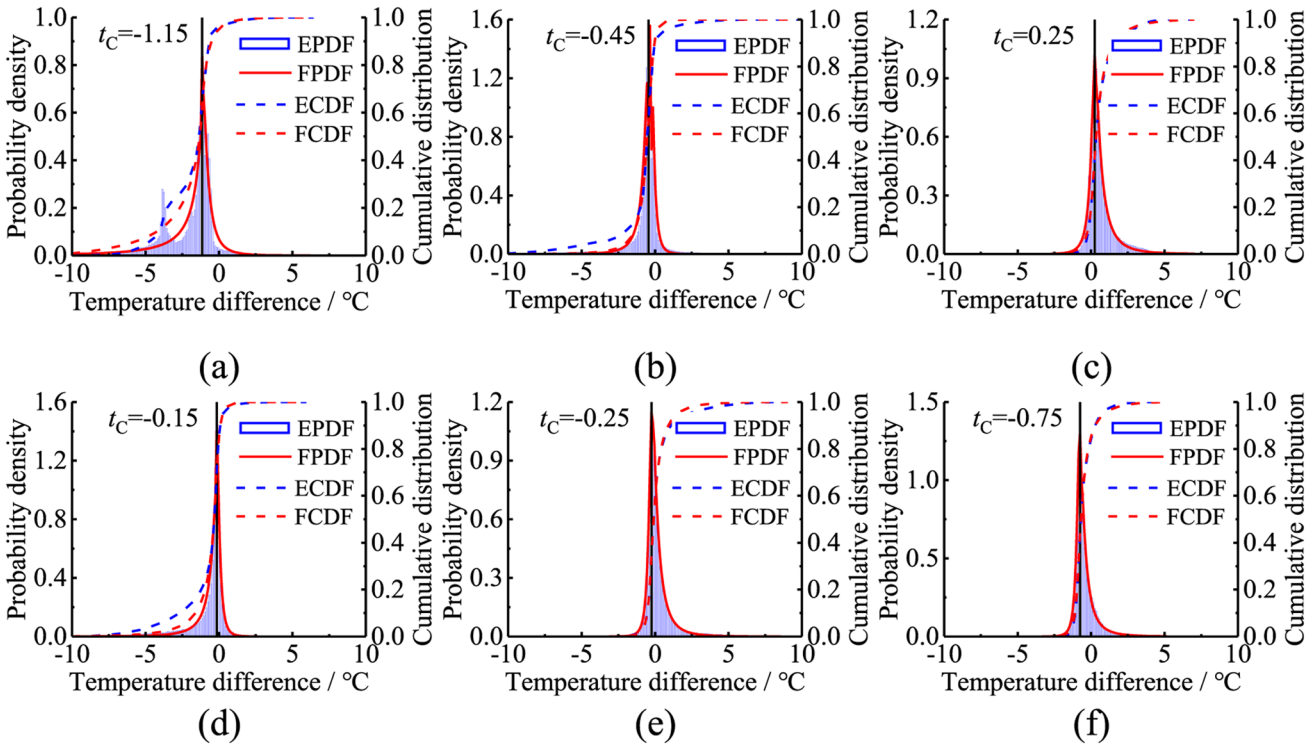

Fig. 8 Probability density distribution for the temperature difference. **a** Diagonal H-shaped member; **b** middle chord member; **c** bottom chord member; **d** vertical H-shaped member; **e** side box-shaped member; **f** middle box-shaped member

the raw data and the fitted curve at the ends. Hence, the first peak is ignored in the assessment of extreme temperatures.

The characteristics of the temperature and temperature difference are analyzed based on three and a half years of temperature data. Accordingly, the probability density distributions of the effective temperature and temperature difference are calculated, which are described using the normal distribution and weighted sum of two lognormal distributions, respectively. Subsequently, extreme conditions with the combination of the effective temperature and temperature difference will be contoured for the structural members in the Dashengguan Bridge.

5 The environmental contours (ECs) for the temperature variation in the Dashengguan Bridge

Environmental contours (ECs) have been widely used to estimate the long-term joint probability distribution of wind and wave parameters for offshore structures [38–40]. As will be shown in this section, ECs can also provide reliable tools for the design and maintenance of bridges. Long-span steel truss arch bridges are designed to withstand the extreme temperature variations predicted for a given site. The critical temperature-induced response is associated with the highest or lowest values of the temperature, which are located at the boundary of the contour. Haselsteiner et al. presented the highest density contour (HDC) method, which defines the EC, encloses the highest density region (HDR) of a given probability density [48]. Based on the long-term field temperature measurements, the ECs for the Dashengguan Bridge are constructed in the remainder of this section to define the extreme temperature variation in typical structural members using the HDC method. Specifically, the ECs without and with the correlation between the effective temperature and temperature difference are mapped for comparison.

5.1 The ECs without correlation

The probability density distributions of effective temperature and temperature difference are shown in Figs. 6 and 8. The ECs for the combination of effective temperature and temperature difference with return periods of 10, 20, and 50 years are obtained using the HDC method. The *N*-year return period means that an environmental state with a probability density less than the corresponding exceedance probability occurs every *N* years, on the average. Note that the correlation between the effective temperature and temperature difference is ignored. The ECs for the six typical structural members are shown in Fig. 9. The top and bottom colors in the color bar represent the

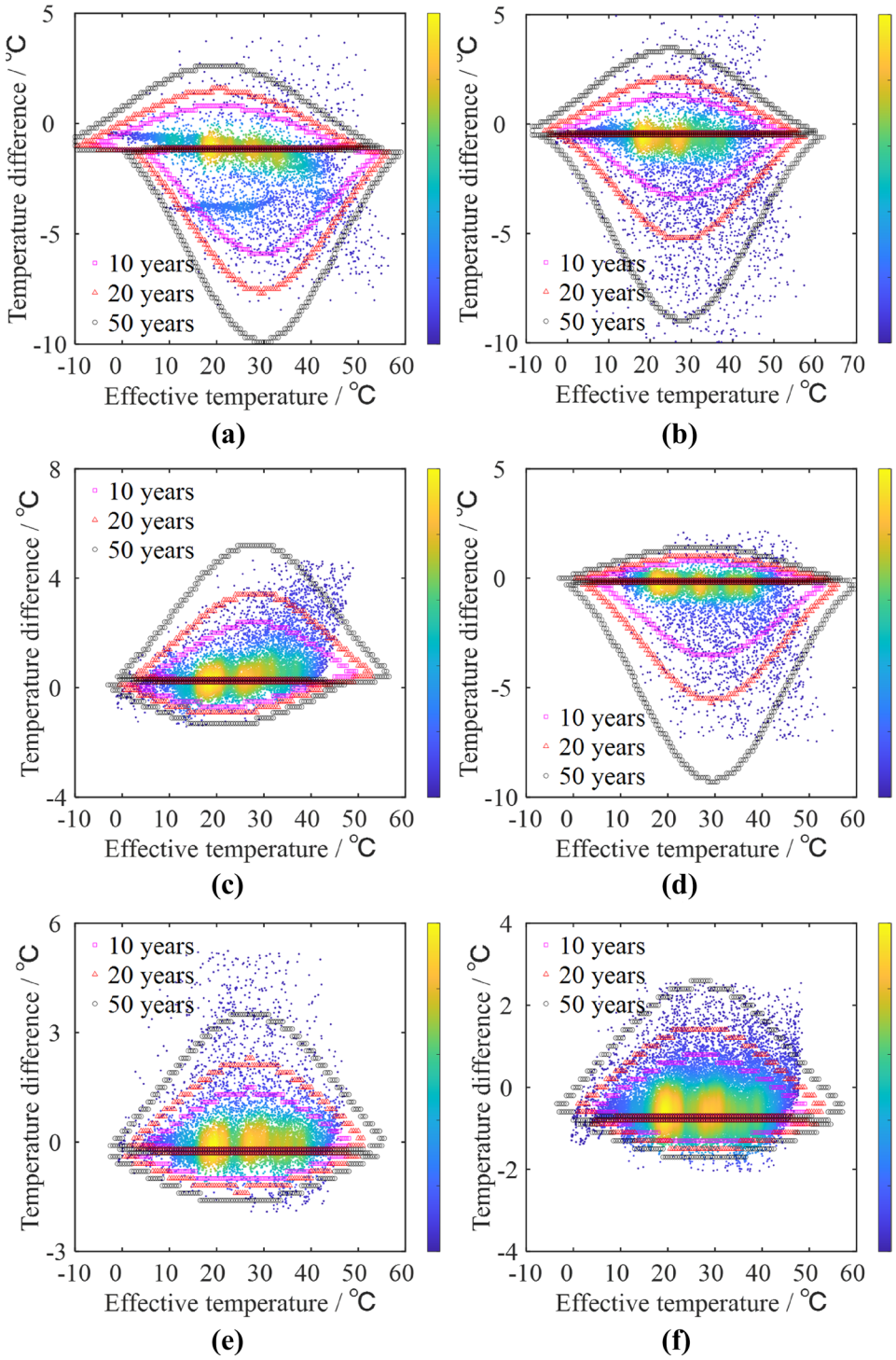

Fig. 9 ECs without the correlation. **a** Diagonal H-shaped member; **b** middle chord member; **c** bottom chord member; **d** vertical H-shaped member; **e** side box-shaped member; **f** middle box-shaped member,

highest and lowest values of the probability density in the figure, respectively. The ECs show the occurrence probability of the temperature variations in the Dashengguan Bridge, which can cause critical temperature-induced responses. The contours are symmetric in the horizontal direction, because the effective temperature is described using the normal distribution. However, the contours cannot describe critical temperature variations accurately, especially the bottom chord member and middle box-shaped member. Thus, the ignored correlation can result in inaccurate assessment of the extreme temperatures in members.

5.2 The ECs considering correlation

The correlation between the effective temperature and temperature difference is mapped in the ECs, aiming at accurately assessing the extreme temperatures in structural members. The temperature difference is modeled as marginal distribution and the effective temperature is modeled as the conditional distribution. The parameters of the conditional distribution are fitted by dividing the temperature difference into several equal classes. Accordingly, the ECs for the combined effective temperature and temperature difference with different return periods can be obtained using the HDC method.

5.2.1 The correlation between the effective temperature and temperature difference

The joint distribution model of the effective temperature, T_E, and temperature difference, T_D, is written as

$$f_{T_E,T_D}(t_E,t_D)=f_{T_D}(t_D)f_{T_E|T_D}(t_E|t_D), \tag{4}$$

where t_D and t_E are the variables of the temperature difference and effective temperature, respectively. Equation (4) consists of a marginal distribution of the temperature difference and a conditional distribution of the effective temperature. The joint distribution model generally gives a good approximation to temperature difference, while this model may overestimate effective temperature at the ends. The lognormal distribution describes the marginal distribution of the temperature difference, T_D, with the PDF given by Eq. (1). Moreover, the probabilistic model of the effective temperature is established as normally distributed variables, conditional on the temperature difference. The conditional distribution of the effective temperature has a PDF is, therefore

$$f_{T_E|T_D}(t_E|t_D)=\frac{1}{\sqrt{2\pi}\sigma_C}\exp\left[-\frac{1}{2\sigma_C^2}(t_E-\mu_C)^2\right], \tag{5}$$

where μ_C and σ_C are the mean and standard deviation of the conditional normal distribution. The mean and standard deviation are conditioned on the temperature difference, which are calculated by

$$\mu_C(t_D)=a_1+a_2e^{a_3t_D}, \tag{6}$$

$$\sigma_C(t_D)=b_1+b_2e^{b_3t_D}, \tag{7}$$

where a_1, a_2, a_3, b_1, b_2, and b_3 are the parameters estimated from the recorded data using nonlinear least-square curve fitting.

The conditional distribution is modelled by fitting a normal distribution with PDF defined by Eq. (5), and the parameters are calculated based on the nonlinear functions defined by Eqs. (6) and (7). The temperature difference is divided into several equal classes. Subsequently, the conditional distribution of the effective temperature is estimated for the different classes. The effects of the bin size can be minor when the number of classes varies in a reasonable range [38]. The fitting parameters for the conditional normal distributions are shown in Fig. 10; the fitting results change little when the number of classes ranges from 6 to 9; therefore, 7 classes are employed in this work. In addition, the conditional normal distributions for different classes are shown in Fig. 11. The normal distribution is seen to be reasonable for all classes. Note that the conditional mean and standard deviation approaches zero for increasing temperature difference, as illustrated in Fig. 10. The contours would not inflate when extrapolating to a higher temperature difference. Therefore, the extreme of effective temperature would not be overestimated infinitely. However, when using the effective temperature as a marginal distribution and the

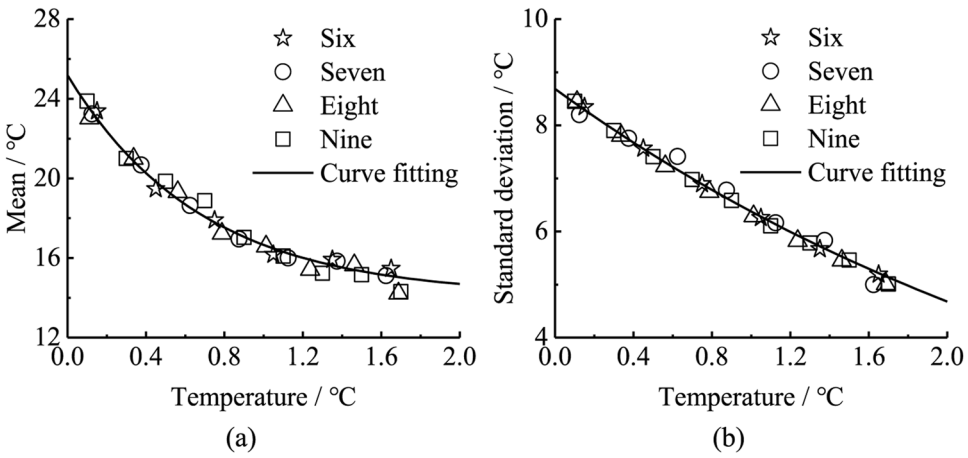

Fig. 10 Nonlinear estimates of the conditional normal distribution parameters. **a** Location parameter; **b** scale parameter

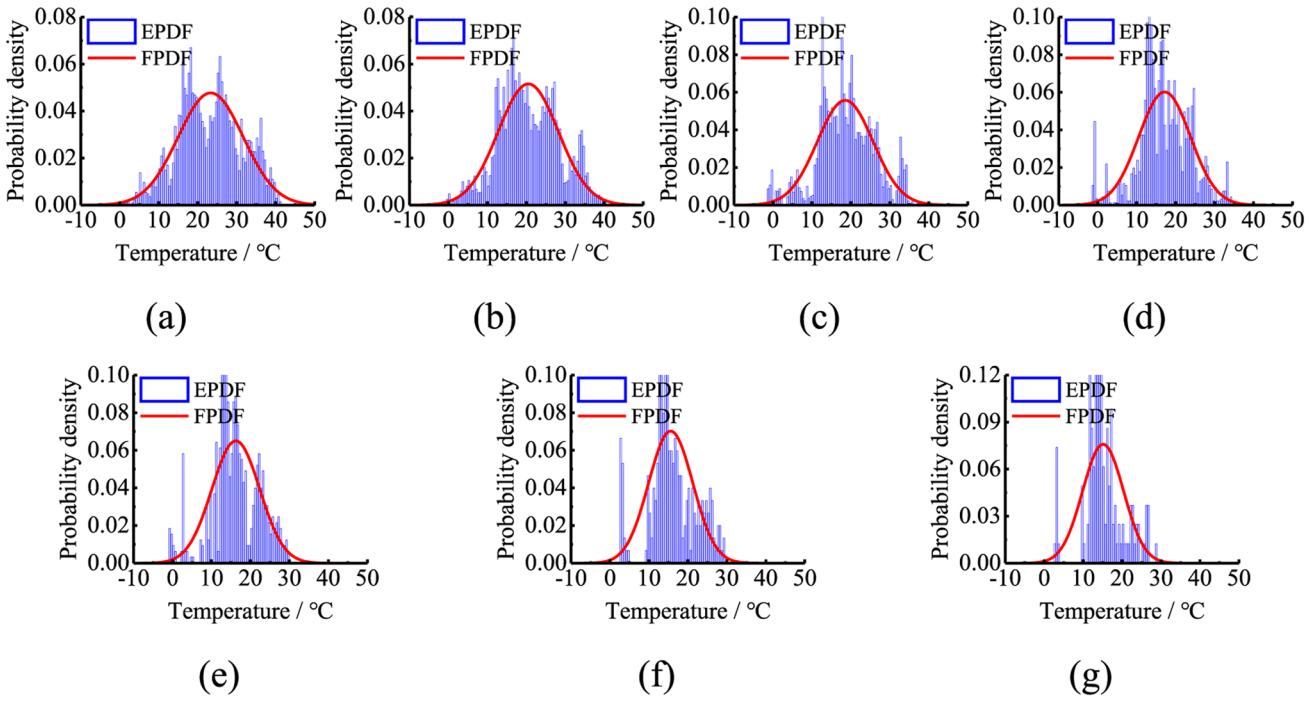

Fig. 11 Conditional distributions of the effective temperature. **a** Class 01; **b** Class 02; **c** Class 03; **d** Class 04; **e** Class 05; (f) Class 06; **g** Class 07

temperature difference as a conditional distribution, the conditional parameters of the temperature difference dramatically increase with the increase in the effective temperature. Thus, the extreme temperature difference corresponding to the higher effective temperature would be larger than that corresponding to the lower effective temperature. This phenomenon is not consistent with the field monitoring data.

5.2.2 The environmental contours (ECs) for structural members

The marginal distributions of temperature difference are shown in Fig. 8. In addition, the parameters of the conditional distribution can be obtained based on Eqs. (6) and (7), as illustrated in Fig. 10. Accordingly, the ECs for the combined effective temperature and temperature difference with return periods of 10, 20, and 50 years can be obtained using the HDC method. The ECs for the six typical structural members are shown in Fig. 12. Note that the top and bottom colors in the color bar represent the highest and lowest value of the probability density in the figure, respectively.

The extremes in the effective temperature and temperature differences vary significantly for different structural members. For structural member facing directly toward the sun, these extremes are much higher, compared to those in the shade, and hence represent the most severe conditions. The middle box-shaped member, which is fully shaded by the deck, generally exhibits the smallest temperature difference. In addition, the geometric size of the box-shaped member under the deck is the largest, resulting in a temperature difference which is relatively small compared to that of other structural members; this difference is neglected. Note that the extreme values of the effective temperature and temperature difference do not occur concurrently.

The uncertainty in the ECs is mainly produced by two sources: (1) the limited temperature measurements and (2) the form of the chosen probability distribution models. The marginal distributions may be affected little by the limited data, whereas the conditional distributions will be significantly affected, as well as the conditional probabilities. Additional long-term monitoring data should be provided for establishing joint distributions to reduce the statistical uncertainty [37]. Note that the number of classes in the conditional distribution analysis has little influence on the uncertainty in the ECs. The selection of probability distribution models for the joint environmental description and the estimation method applied for the determination of distribution parameters also influences the uncertainty. The normal distribution is employed to represent the effective temperature, which provides good agreement, as shown in Fig. 11. Nevertheless, significant discrepancies are observed between the recorded data and the fitted distribution in Fig. 11f, g. The normal distribution may overestimate the probabilities in the tails, which can result in an overestimation of the effective temperature. Moreover, modeling the ECs with the temperature difference as marginal distribution and the

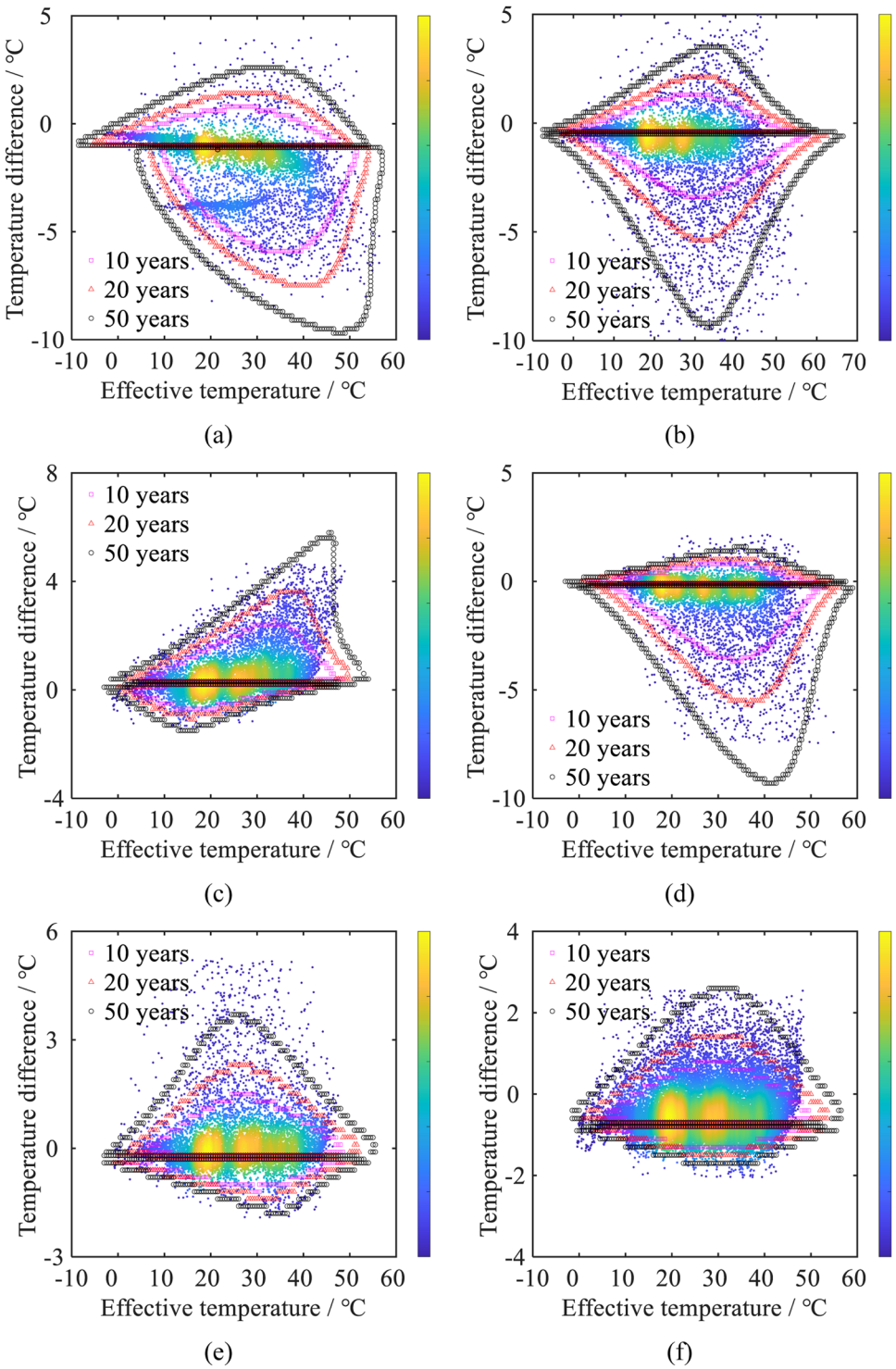

Fig. 12 ECs considering the correlation. **a** Diagonal H-shaped member; **b** middle chord member; **c** bottom chord member; **d** vertical H-shaped member; **e** side box-shaped member; **f** middle box-shaped member

effective temperature as the conditional distribution is good practice, because the temperature difference has larger influences on structural responses than the effective temperature [24].

The ignored correlation between the effective temperature and temperature difference can result in inaccurate assessment of the extreme temperatures in members. The ECs without correlation provide underestimation of the extreme temperatures in members, which may pose a danger to bridge safety and serviceability. In addition, concurrently employing the extreme effective temperature and extreme temperature difference provides overestimation of the temperature extremes, which could lead to expensive over-designs. Hence, the ECs considering correlation

would provide critical information for the design and maintenance of long-span bridges during life cycles, especially for structural members facing directly toward the sun. In addition, the negative extreme temperature difference is dominant in the structural member directly exposed to solar radiation, indicating that the temperature of the west-facing plate is higher than that of the east-facing plate, whereas the opposite situation occurs in the shaded member. The study leads to more accurate estimation of the temperature extremes in long-span steel truss arch bridges, which are of great importance for proper design and maintenance of bridges.

6 Conclusion

Bridges are designed to withstand the extreme temperature variations predicted for a given site. Hence, the joint probability distribution for the temperature variation, which considers the correlation between the effective temperature and temperature difference, would provide critical information for the design and maintenance of long-span bridges. In this study, the characteristics of the temperature and temperature difference were analyzed based on three and a half years of temperature data. Accordingly, the probability density distributions of the effective temperature and temperature difference were described using the normal distribution and weighted sum of two lognormal distributions, respectively. Then, the environmental contours (ECs) with the return period of 10, 20, and 50 years were presented using the highest density contour (HDC) method, which revealed the extreme temperature variations in the bridge. The following conclusions can be drawn from this study.

- The probability density distribution of the effective temperature was described using a normal distribution, while the combination of two lognormal distributions was employed to describe the temperature difference.
- The ECs provided a condensed representation of field temperature measurements and a better representation of extreme conditions. The EC with the temperature difference as marginal distribution and the effective temperature as the conditional parameter was shown to be a good approximation for the extreme temperature difference, whereas it may overestimate the effective temperature in the tails.
- The effective temperature and temperature difference in structural members directly exposed to solar radiation varied significantly, whereas the temperature difference of the shaded structural member was neglected. In addition, the extreme values of the effective temperature and temperature difference did not occur concurrently.

This study leads to more accurate estimation of the temperature extremes in long-span steel truss arch bridges, which are of great importance for proper design and maintenance of bridges. In addition, the results can provide reliable references for the design and maintenance of similar steel truss bridges at the adjacent site.

Acknowledgements This research was supported by the National Natural Science Foundation of China (Grant Nos. 51722804 and 51978155), the National Ten Thousand Talent Program for Young Top-notch Talents (Grant No. W03070080), the Jiangsu Key Research and Development Plan (Grant No. BE2018120), the Postgraduate Research and Practice Innovation Program of Jiangsu Province (Grant No. KYCX19_0095) and the National Construction of High-level University Public Graduate Project (Grant No. CSC201906090075). This support is gratefully acknowledged. The authors also thank the China Academy of Railway Sciences and the China Railway Shanghai Group Company Limited for providing the long-term monitoring data for the Dashengguan Bridge.

Author contributions Q-XZ: Investigation, methodology, visualization, writing. HW: conceptualization, funding acquisition. Z-DX: Validation. BFSJr.: Supervision, review. J-XM: Editing. Z-HG: Data curation.

Funding This research was supported by the National Natural Science Foundation of China (Grant No. 51722804 and 51978155), the National Ten Thousand Talent Program for Young Top-notch Talents (Grant No. W03070080), the Jiangsu Key Research and Development Plan (Grant No. BE2018120), the Postgraduate Research and Practice Innovation Program of Jiangsu Province (Grant No. KYCX19_0095) and the National Construction of High-level University Public Graduate Project (Grant No. CSC201906090075).

Code availability Some code used during the study is available from the corresponding author by request, e.g., the code for the highest density contour (HDC) method.

Data availability Some data, models, or code used during the study are available from the corresponding author by request, including some field monitoring data shown in Fig. 5 and the code for the highest density contour (HDC) method.

Declarations

Conflict of interest The authors declare that there is no conflict of interest regarding the publication of this paper.

Availability of data and material Some data used during the study is available from the corresponding author by request, e.g., the field monitoring data shown in Fig. 5.

References

1. Han QH, Ma Q, Xu J et al (2020) Structural health monitoring research under varying temperature condition: a review. J Civ Struct Health Monit. https://doi.org/10.1007/s13349-020-00444-x
2. Jesus A, Brommer P, Westgate R et al (2019) Bayesian structural identification of a long suspension bridge considering temperature and traffic load effects. Struct Health Monit 18(4):1310–1323. https://doi.org/10.1177/1475921718794299

3. Teng J, Tang DH, Hu WH et al (2020) Mechanism of the effect of temperature on frequency based on long-term monitoring of an arch bridge. Struct Health Monit 1475921720931370:1–22. https://doi.org/10.1177/1475921720931370
4. Xia Q, Zhou LM, Zhang J (2018) Thermal performance analysis of a long-span suspension bridge with long-term monitoring data. J Civ Struct Health Monit 8(4):543–553. https://doi.org/10.1007/s13349-018-0299-y
5. Hossain T, Segura S, Okeil AM (2020) Structural effects of temperature gradient on a continuous prestressed concrete girder bridge: analysis and field measurements. Struct Infrastruct Eng. https://doi.org/10.1080/15732479.2020.1713167
6. Kromanis R, Kripakaran P (2016) SHM of bridges: characterising thermal response and detecting anomaly events using a temperature-based measurement interpretation approach. J Civ Struct Health Monit 6(2):237–254. https://doi.org/10.1007/s13349-016-0161-z
7. Liu Y, Qian ZD, Hu J et al (2018) Temperature behavior and stability analysis of orthotropic steel bridge deck during gussasphalt pavement paving. J Bridge Eng 23(1):04017117. https://doi.org/10.1061/(ASCE)BE.1943-5592.0001163
8. Xu YL, Chen B, Ng CL et al (2010) Monitoring temperature effect on a long suspension bridge. Struct Control Health Monit 17(6):632–653. https://doi.org/10.1002/stc.340
9. Wang D, Liu YM, Liu Y (2018) 3D temperature gradient effect on a steel-concrete composite deck in a suspension bridge with field monitoring data. Struct Control Health Monit 25(7):e2179. https://doi.org/10.1002/stc.2179
10. Fujino Y (2002) Vibration, control and monitoring of long-span bridges-recent research, developments and practice in Japan. J Constr Steel Res 58(1):71–97. https://doi.org/10.1016/S0143-974X(01)00049-9
11. Wong KY (2004) Instrumentation and health monitoring of cable-supported bridges. Struct Control Health Monit 11(2):91–124. https://doi.org/10.1002/stc.33
12. Ko JM, Ni YQ (2005) Technology developments in structural health monitoring of large-scale bridges. Eng Struct 27(12):1715–1725. https://doi.org/10.1016/j.engstruct.2005.02.021
13. Li H, Ou JP (2016) The state of the art in structural health monitoring of cable-stayed bridges. J Civ Struct Health Monit 6(1):43–67. https://doi.org/10.1007/s13349-015-0115-x
14. Spencer BF Jr, Jo H, Mechitov KA et al (2016) Recent advances in wireless smart sensors for multi-scale monitoring and control of civil infrastructure. J Civ Struct Health Monit 6(1):17–41. https://doi.org/10.1007/s13349-015-0111-1
15. Mao JX, Wang H, Feng DM et al (2018) Investigation of dynamic properties of long-span cable-stayed bridges based on one-year monitoring data under normal operating condition. Struct Control Health Monit 25(5):e2146. https://doi.org/10.1002/stc.2146
16. Xu YL (2018) Making good use of structural health monitoring systems of long-span cable-supported bridges. J Civ Struct Health Monit 8(3):477–497. https://doi.org/10.1007/s13349-018-0279-2
17. Zhou Y, Sun LM (2019) Insights into temperature effects on structural deformation of a cable-stayed bridge based on structural health monitoring. Struct Health Monit 18(3):778–791. https://doi.org/10.1177/1475921718773954
18. Abid SR, Mussa F, Tayşi N et al (2018) Experimental and finite element investigation of temperature distributions in concrete-encased steel girders. Struct Control Health Monit 25(1):e2042. https://doi.org/10.1002/stc.2042
19. Yang DH, Yi TH, Li HN et al (2018) Monitoring and analysis of thermal effect on tower displacement in cable-stayed bridge. Measurement 115:249–257. https://doi.org/10.1016/j.measurement.2017.10.036
20. Xia Y, Hao H, Zanardo G et al (2006) Long term vibration monitoring of an RC slab: temperature and humidity effect. Eng Struct 28(3):441–452. https://doi.org/10.1016/j.engstruct.2005.09.001
21. Xu ZD, Wu ZS (2007) Simulation of the effect of temperature variation on damage detection in a long-span cable-stayed bridge. Struct Health Monit 6(3):177–189. https://doi.org/10.1177/1475921707081107
22. Giles RK, Spencer BF Jr (2015) Development of a long-term, multimetric structural health monitoring system for a historic steel truss swing bridge. Newmark Structural Engineering Laboratory. University of Illinois, Urbana-Champaign
23. Huang HB, Yi TH, Li HN et al (2018) New representative temperature for performance alarming of bridge expansion joints through temperature-displacement relationship. J Bridg Eng 23(7):04018043. https://doi.org/10.1061/(ASCE)BE.1943-5592.0001258
24. Zhu QX, Wang H, Mao JX et al (2020) Investigation of temperature effects on steel-truss bridge based on long-term monitoring data: case Study. J Bridg Eng 25(9):05020007. https://doi.org/10.1061/(ASCE)BE.1943-5592.0001593
25. Zhu JS, Meng QL (2017) Effective and fine analysis for temperature effect of bridges in natural environments. J Bridge Eng 22(6):04017017. https://doi.org/10.1061/(ASCE)BE.1943-5592.0001039
26. Ding YL, Zhou GD, Li AQ et al (2012) Thermal field characteristic analysis of steel box girder based on long-term measurement data. Int J Steel Struct 12(2):219–232. https://doi.org/10.1007/s13296-012-2006-x
27. Tong M, Tham LG, Au FT (2002) Extreme thermal loading on steel bridges in tropical region. J Bridg Eng 7(6):357–366. https://doi.org/10.1061/(ASCE)1084-0702(2002)7:6(357)
28. Zhou GD, Yi TH, Chen B et al (2017) A generalized Pareto distribution–based extreme value model of thermal gradients in a long-span bridge combining parameter updating. Adv Struct Eng 20(2):202–213. https://doi.org/10.1177/1369433216660010
29. Wang H, Zhu QX, Zou ZQ et al (2020) Temperature distribution analysis of steel box-girder based on long-term monitoring data. Smart Struct Syst 25(5):593–604. https://doi.org/10.12989/sss.2020.25.5.593
30. Liu J, Liu YJ, Jiang L et al (2019) Long-term field test of temperature gradients on the composite girder of a long-span cable-stayed bridge. Adv Struct Eng 22(13):2785–2798. https://doi.org/10.1177/1369433219851300
31. Zhou LR, Xia Y, Brownjohn JM et al (2016) Temperature analysis of a long-span suspension bridge based on field monitoring and numerical simulation. J Bridg Eng 21(1):04015027. https://doi.org/10.1061/(ASCE)BE.1943-5592.0000786
32. Gottsäter E, Ivanov OL, Molnár M et al (2017) Simulation of thermal load distribution in portal frame bridges. Eng Struct 143:219–231. https://doi.org/10.1016/j.engstruct.2017.04.012
33. Giussani F (2009) The effects of temperature variations on the long-term behavior of composite steel-concrete beams. Eng Struct 31(10):2392–2406. https://doi.org/10.1016/j.engstruct.2009.05.014
34. Li QY, Gao Z, Moan T (2016) Modified environmental contour method for predicting long-term extreme responses of bottom-fixed offshore wind turbines. Mar Struct 48:15–32. https://doi.org/10.1016/j.marstruc.2016.03.003
35. Vanem E (2017) A comparison study on the estimation of extreme structural response from different environmental contour methods. Mar Struct 56:137–162. https://doi.org/10.1016/j.marstruc.2017.07.002
36. Haselsteiner AF, Lehmkuhl J, Pape T et al (2019) ViroCon: A software to compute multivariate extremes using the environmental contour method. SoftwareX 9:95–101. https://doi.org/10.1016/j.softx.2019.01.003

37. Saranyasoontorn K, Manuel L (2006) Design loads for wind turbines using the environmental contour method. J SolEnergy Eng 128(4):554–561. https://doi.org/10.1115/1.2346700
38. Li L, Gao Z, Moan T (2015) Joint distribution of environmental condition at five European offshore sites for design of combined wind and wave energy devices. J Offshore Mech Arctic Eng. doi 10(1115/1):4029842
39. Karmakar D, Bagbanci H, Guedes Soares C (2016) Long-term extreme load prediction of spar and semisubmersible floating wind turbines using the environmental contour method. J Offshore Mech Arctic Eng. doi 10(1115/1):4032099
40. Velarde J, Vanem E, Kramhøft C et al (2019) Probabilistic analysis of offshore wind turbines under extreme resonant response: Application of environmental contour method. Appl Ocean Res 93:101947. https://doi.org/10.1016/j.apor.2019.101947
41. Raed K, Teixeira AP, Soares CG (2020) Uncertainty assessment for the extreme hydrodynamic responses of a wind turbine semi-submersible platform using different environmental contour approaches. Ocean Eng 195:106719. https://doi.org/10.1016/j.oceaneng.2019.106719
42. Van de Lindt JW, Niedzwecki JM (2000) Environmental contour analysis in earthquake engineering. Eng Struct 22(12):1661–1676. https://doi.org/10.1016/S0141-0296(99)00114-5
43. Lystad TM, Fenerci A, Øiseth O (2020) Buffeting response of long-span bridges considering uncertain turbulence parameters using the environmental contour method. Eng Struct 213:110575. https://doi.org/10.1016/j.engstruct.2020.110575
44. Xia Y, Chen B, Zhou XQ et al (2013) Field monitoring and numerical analysis of Tsing Ma Suspension Bridge temperature behavior. Struct Control Health Monit 20(4):560–575. https://doi.org/10.1002/stc.515
45. Liu Y, Qian ZD, Hu HZ (2016) Thermal field characteristic analysis of steel bridge deck during high-temperature asphalt pavement paving. KSCE J Civ Eng 20(7):2811–2821. https://doi.org/10.1007/s12205-016-0027-2
46. Ni YQ, Hua XG, Wong KY et al (2007) Assessment of bridge expansion joints using long-term displacement and temperature measurement. J Perform Constr Facil 21(2):143–151. https://doi.org/10.1061/(ASCE)0887-3828(2007)21:2(143)
47. Deng Y, Li AQ, Liu Y et al (2018) Investigation of temperature actions on flat steel box girders of long-span bridges with temperature monitoring data. Adv Struct Eng 21(14):2099–2113. https://doi.org/10.1177/1369433218766946
48. Haselsteiner AF, Ohlendorf JH, Wosniok W et al (2017) Deriving environmental contours from highest density regions. Coast Eng 123:42–51. https://doi.org/10.1016/j.coastaleng.2017.03.002